

Crystal and magnetic structure of Ca_2RuO_4 : Magnetoelastic coupling and the metal-insulator transition

M. Braden

*Forschungszentrum Karlsruhe, INFP, Postfach 3640, 76021 Karlsruhe, Germany
and Laboratoire Leon Brillouin, CE-Saclay, 91191 Gif-sur-Yvette, France*

G. André

Laboratoire Leon Brillouin, CE-Saclay, 91191 Gif-sur-Yvette, France

S. Nakatsuji and Y. Maeno

Department of Physics, Kyoto University, Kyoto 606-8502, Japan

(Received 4 December 1997)

The crystal and magnetic structure of Ca_2RuO_4 (CRO) has been studied by powder neutron diffraction. CRO was synthesized in two different modifications (stoichiometric and containing excess oxygen) whose crystal structures are, in spite of strong differences in the lattice constants, closely related. Both structures are derived from the ideal K_2NiF_4 structure type by a rotation of the RuO_6 octahedra around the long axis, combined with a tilt around an axis lying in the RuO_2 plane. The orientation of the tilt axis seems to distinguish the two room-temperature symmetries; the excess oxygen compound is characterized by a smaller tilt angle and shorter Ru-O in-plane bond distances. Stoichiometric CRO undergoes large structural changes on cooling, though no symmetry change was detected. In contrast, the excess oxygen containing compound undergoes a first-order structural phase transition accompanied by a change from metallic to insulating behavior in the electric resistivity. Both compounds exhibit antiferromagnetic order below 110–150 K; for the stoichiometric sample, the onset of magnetic order is associated with several structural anomalies. [S0163-1829(98)04526-3]

I. INTRODUCTION

The discovery of superconductivity in the layered perovskite Sr_2RuO_4 (SRO) (Ref. 1) stimulated a great deal of research effort due to its close structural resemblance with the original high- T_c cuprate. The electronic properties of SRO indicate a two-dimensional (2D)-Fermi liquid under the influence of electronic correlations.^{2,3} Whether these correlations are essential for the understanding of SRO or not is widely discussed in the literature.^{4,5} A rather large U/W ratio (the ratio of the on-site Coulomb repulsion and the one-particle bandwidth) demonstrates that, in spite of its highly metallic conductivity, SRO is close to a Mott transition.³

The mechanism of superconductivity in SRO might give further insight to that of the cuprates. Rice and Sigrist⁶ proposed a triplet pairing induced by ferromagnetic correlations. The first assumption of a nearby ferromagnetic instability suggested by the ferromagnetic ordering in the perovskite SrRuO_3 , was more recently confirmed by a general band-structure analysis of the known perovskite related ruthenates.^{4,5} The recent announcement of a much higher superconducting T_c in the Cu-doped double perovskite $\text{Sr}_2\text{YRu}_{1-x}\text{Cu}_x\text{O}_6$ promises further relevance of the ruthenates in the context of high-temperature superconductivity.⁷

Another compound closely related to SRO is the Ca analog Ca_2RuO_4 (CRO), whose synthesis was recently reported.^{8,9} In contrast to the ferromagnetic instability suggested for SRO, CRO exhibits antiferromagnetic ordering with only a weak ferromagnetic component induced by spin canting.⁸ The first magnetic studies clearly exclude a ferro-

magnetic transition. In addition, CRO is found to be a Mott insulator which was interpreted as being due to an enhanced U/W ratio. Assuming a comparable U value, this necessitates a smaller band width due to either a smaller Ru- d O- p orbital overlap or a pronounced structural distortion. That the structure of CRO is rather complicated was already suggested by previous reports: Nakatsuji *et al.*⁸ have synthesized two distinct polycrystalline samples, whose lattice constants do not well agree with those of the single crystal analyzed by G. Cao *et al.*⁹

We have analyzed polycrystalline CRO samples by powder neutron diffraction. The structure of CRO is found to be strongly distorted; furthermore, these distortions cause enormous structural variations with temperature and a high sensitivity to stoichiometry.

II. EXPERIMENTAL

As reported previously,⁸ CRO can be synthesized in two distinct phases, the main difference being the value of the long lattice constant (c in space group $I4/mmm$). We have prepared polycrystalline samples of both phases according to the procedures described in Ref. 8. Thermogravimetric analyses and the fact that the sample with the longer c axis is obtained after annealing 50 h in air at 400 °C indicate that this latter sample has an oxygen excess; throughout the paper, we will label the two compounds stoichiometric CRO (S-CRO) (short $c \sim 11.94$ Å) and excess oxygen CRO (O-CRO) (long $c \sim 12.35$ Å). S-CRO is partially recovered from O-CRO by annealing at 900 °C in air and quickly cooling.

Neutron-diffraction experiments have been performed us-

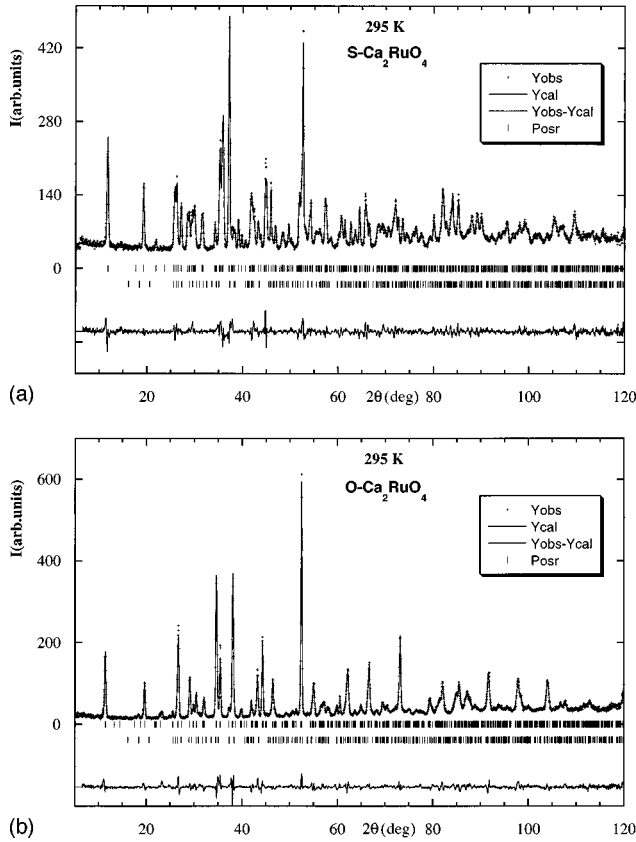


FIG. 1. Diffraction patterns obtained with the high-resolution diffractometer 3T.2 for S-CRO (top) and O-CRO (bottom) together with the corresponding calculated profiles. The upper row of the vertical bars indicates the positions of the Bragg reflections belonging to the main CRO phases and the lower row those of the impurity CaRuO_3 phase.

ing two diffractometers installed at the Orphée reactor. The high-resolution diffractometer 3T.2 ($\lambda = 1.227 \text{ \AA}$) was used to obtain data sets extending to rather high Q values, which enabled a detailed structure determination. This diffractometer uses a Ge (3 3 5) monochromator and tight collimations: $10'$ in front of the monochromator and $10'$ in front of the 20 detectors. Both samples were measured at room temperature and at 11 K. The measured diffraction patterns at room temperature together with the calculated ones are shown in Fig. 1. The results of the structure refinements are given in Table I. In order to examine the magnetic ordering and the temperature dependences of the main structural parameters a larger number of patterns were taken on the G4.1 diffractometer between 1.5 and 295 K. The G4.1 instrument is placed at a cold neutron guide and uses a focusing pyrolytic graphite (002) monochromator ($\lambda = 2.427 \text{ \AA}$); a bank of 800 detectors further increases its efficiency. As an example we show in Fig. 2 two patterns obtained on the S-CRO together with the profiles calculated using the Rietveld method. The high flux of G4.1 allowed us to collect patterns at several temperatures on cooling and then finely spaced data points on heating with a temperature step of approximately 5 K for both samples. Magnetic susceptibility and resistivity were measured as described in Ref. 8.

III. RESULTS AND DISCUSSION

A. Crystal structure of S-CRO

That S-CRO has not the ideal K_2NiF_4 structure is already demonstrated by the strong orthorhombic distortion at room temperature, which further increases on cooling. Also, the temperature dependence of the lattice constants and the volume, shown in Fig. 3, is far from normal: the volume even increases on cooling. The orthorhombic distortion and the extremely large and anisotropic thermal expansions indicate a dominant structural distortion.

Structural distortions are of course not at all unusual in a perovskite-related compound; they are frequently due to a rotation of the octahedra and indeed such distortions are observed in the related compounds Sr_2IrO_4 (Ref. 10) and Sr_2RhO_4 (Ref. 11) which possess the $I4_1/acd$ tetragonal symmetry corresponding to a rotation of the octahedron around the long axis (note that the long lattice parameter is doubled compared with the K_2NiF_4 lattice). SRO, which remains undistorted down to low temperatures¹² is rather close to the rotational instability as evidenced by the measurements of the corresponding phonon modes.¹³ The orthorhombic distortion in S-CRO indicates, however, a different distortion type. The octahedra rotation around c may also lead to an orthorhombic symmetry, similar to that found in Gd_2CuO_4 (Ref. 14) in space group $Acam$ (standard setting $Cmca$, where a corresponds to the long axis, which is not doubled; throughout the paper we will use nonstandard settings when necessary in order to keep the long axis always as c). However, in this symmetry the orthorhombic distortion is only weakly coupled to the rotation angle and, therefore, remains very small. Another isostructural material, La_2CuO_4 , exhibits a similar though still much smaller orthorhombic splitting than S-CRO. In La_2CuO_4 , the low-temperature phase is characterized by a tilt of the octahedra around an axis lying in the plane (space group $Cmca$, where b represents the long axis).¹⁵ Throughout the paper we will call “tilt” distortions deformations where the octahedra are tilted around an axis lying in the RuO_2 (or CuO_2) planes and “rotational” distortions those where the octahedra are turned around the long axis (c in $I4/mmm$). Attempts to describe the measured S-CRO patterns by the La_2CuO_4 structure type remained unsatisfying, indicating another distortion element. A sensible approach is to combine the two distortion types, in order to describe the distortion in CRO.

The symmetry reductions from the ideal K_2NiF_4 structure (space group $I4/mmm$) together with the corresponding octahedra rotations or tilts are summarized in Fig. 4, with the restriction to those low-symmetry space groups which do not require a doubling of the long axis. The well studied tilt transitions in La_2CuO_4 and other T -phase cuprates lead to three space-group symmetries all with $\sqrt{2}a \times \sqrt{2}a \times c$ lattices, distinguished by the orientation of the tilt axis:¹⁶ in $Abma$ or $Bmab$ (standard setting $Cmca$, with b the long axis) it is parallel to an octahedron edge, in $P4_2/nm$ it is parallel to a diagonal and in $Pccn$ to any other axis lying in the planes. The first two phases are commonly called low temperature orthorhombic (LTO) and low temperature tetragonal (LTT), respectively. The LTO symmetry may be further reduced by rotating the entire tilted octahedron around the long axis.

TABLE I. Results of the structural refinements with the data obtained on the high-resolution diffractometer 3T.2. ϵ designates the orthorhombic strain. In space group $P2_1/c$ there are twice as many sites in the asymmetric unit as in space group $Pbca$. However, the loss of the corresponding symmetry operator, Eq. (1), yields significant differences only for three parameters, Ca- x , Ca- y , and O(1)- z , where the two values are separated in the table by the slash. All other additional parameters were constrained corresponding to Eq. (1). U_{\parallel} and U_{\perp} denote the mean-square atomic displacements parallel and perpendicular to the Ru-O bonds.

	S-CRO 295 K <i>Pbca</i>	S-CRO 11 K <i>Pbca</i>	O-CRO 11 K <i>Pbca</i>	O-CRO 295 K $P2_1/c$
a (Å)	5.4097(3)	5.3877(2)	5.4074(8)	5.3292(6)
b (Å)	5.4924(4)	5.6323(3)	5.5150(10)	5.3194(4)
c (Å)	11.9613(6)	11.7463(5)	11.9052(16)	12.3719(8)
Vol (Å ³)	355.4	356.45	355.0	350.72
ϵ	0.0076	0.0222	0.0099	0.0093
β (deg)	/	/	/	90.04(2)
R_{wp} (%)	6.85	7.26	8.55	8.99
Ca x	0.0086(6)	0.0021(5)	0.0057(9)	0.0202(2)/0.5095(26)
y	0.0474(6)	0.0593(4)	0.0486(9)	0.0138(30)/0.5188(30)
z	0.3518(2)	0.3525(2)	0.3516(4)	0.3475(2)
U_{iso}	0.0093(9)	0.0040(6)	0.0040	0.0086(9)
Ru U_{iso}	0.0038(6)	0.0033(6)	0.0033	0.0020(8)
O(1) x	0.1961(4)	0.1952(4)	0.1942(7)	0.1882(8)
y	0.3013(5)	0.3005(4)	0.2996(7)	0.3062(6)
z	0.0234(2)	0.0272(2)	0.0225(3)	0.0/0.0137(9)
U_{\perp} -plane	0.0140(14)	0.0047(10)	0.0047	0.0081(9)
U_{\parallel} -plane	0.0060(6)	0.0014(9)	0.0014	0.0055(6)
$U_{\text{long-axis}}$	0.0144(14)	0.0080(15)	0.0080	0.0237(21)
O(2) x	-0.0576(3)	-0.0692(3)	-0.0611(6)	-0.0295(8)
y	-0.0154(5)	-0.0212(4)	-0.0152(8)	-0.0062(11)
z	0.1646(2)	0.1645(2)	0.1667(3)	0.1650(2)
U_{\perp}	0.0125(10)	0.0045(9)	0.0045	0.0113(12)
U_{\parallel}	0.0093(9)	0.0002(10)	0.0002	0.0045(11)

This corresponds to a condensation of a Y_2^+ phonon mode (corresponding to the $Cmca$ setting) and may result in a continuous phase transition.¹⁷ The space group of this ‘‘tilt plus rotation’’ distortion is $Pbca$ (in this space group the settings corresponding to an even transmutation of the directions are identical; so, c corresponds to the long axis). An important feature of the $Pbca$ symmetry is the existence of only one in-plane oxygen position [O(1)], therefore, all in plane oxygens possess the same distance to the planes formed by the Ru atoms. One may reach the $Pbca$ structure also in the inverted way: first a reduction of the symmetry according to the rotational transition in space group $Acam$ and second the shift of the O(1) sites parallel to the long axis again with the constraint that all O(1) sites have the same distance to the RuO_2 planes.

The fits of the measured diffraction patterns with the $Pbca$ structural model yield a good agreement for both temperatures, see for example Fig. 1(a). The structural parameters are listed in Table I. The low-temperature structure is further presented in Fig. 5 in the form of an ORTEP plot, which clearly demonstrates the enormous structural distortion present in S-CRO. It is obvious that the observed patterns do not show the experimental resolution but an intrinsic broadening; this can also be seen in the comparison of the x-ray

diffraction patterns for both CRO phases and SRO presented in Ref. 8. One should note that an exceptional quality of the SRO sample was achieved in that work by crushing single crystals. The anisotropic broadening was taken into account in our refinements by orthorhombic microstrains.¹⁸ The fact that these strains are strongest along b and weakest along a reflects well the thermal expansion of S-CRO (see Fig. 3). This may indicate some small stoichiometry fluctuations which nevertheless have an impact on the distortion and the lattice parameters. Both CRO phases show some impurity peaks which are partially due to the CaRuO_3 perovskite. In the case of S-CRO this perovskite phase represents only 2 vol. %. Nevertheless, it was taken into consideration during the refinements by fitting only its scale factor using the structural parameters given in Ref. 19.

Table II resumes some characteristic bond distances and angles obtained for the S-CRO sample. The angle describing the rotation of the RuO_6 octahedron around the c axis is rather large, $\phi = 11.8^\circ$, and shows no temperature dependence. Similar values are observed in Sr_2RhO_4 (Ref. 11) and Sr_2IrO_4 (Ref. 10), where also little temperature dependence below room temperature is found. The rotational distortion appears to be the main structural instability in these $4d$ and $5d$ compounds in agreement with the analysis of the lattice dynamics in SRO.¹³ A corresponding phase transition in S-

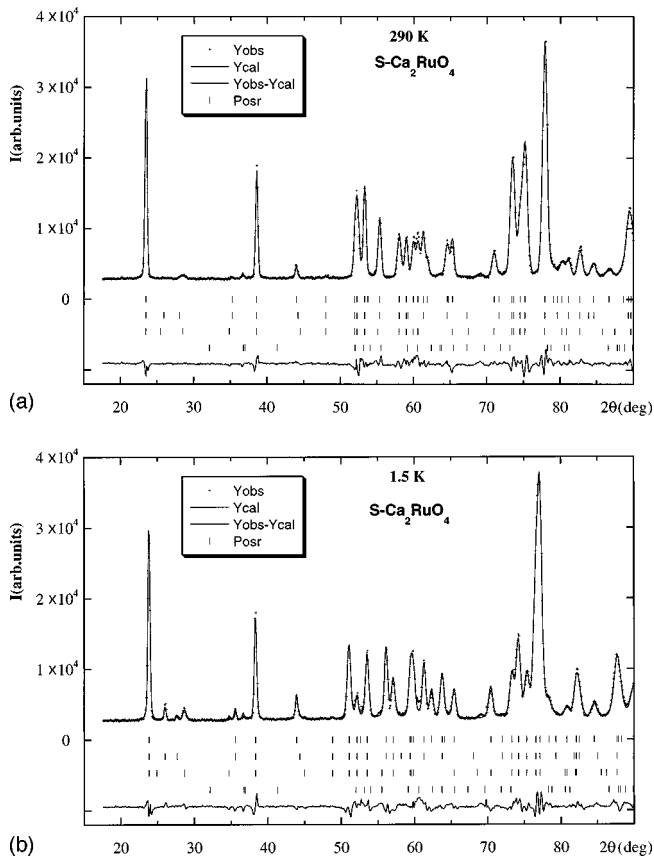


FIG. 2. Diffraction patterns obtained on the high flux diffractometer *G4.1* with S-CRO together with the calculated profiles taking into account the structural phase of S-CRO in space group *Pbca*, the magnetic phases corresponding to the *A*-centered and *B*-centered magnetic modes and the CaRuO_3 impurity phase. The four rows of vertical bars indicate the positions of the Bragg reflections corresponding to these four phases in the sequence given above.

CRO should, if at all, occur at elevated temperatures and might possess strong order-disorder character. The role of this distortion for the electronic properties of all these compounds still needs to be elucidated. However, the phase diagram of $\text{Sr}_2\text{Ru}_{1-x}\text{Ir}_x\text{O}_4$ indicates a close coupling.^{20,21} The latter compounds show metallic behavior only for low Ir concentrations; the structural rotational transition occurring for elevated concentrations seems to induce nonmetallic properties.

The tilt angle of the octahedra can be calculated using either the apical oxygen [O(2)] or the basal planes. The basal planes tilt around an axis shifted from the *b* axis by ϕ ; the tilt angle between the octahedron basal planes and the *a*, *b* planes, $\theta\text{-O}(1)$, increases from 11.2° at room temperature to 12.7° at 11 K. The tilt of the octahedron results in a shift of the O(2) site perpendicular to *c*; the direction of this shift is almost parallel to *a*, the deviation is due to the octahedron rotation around the long axis and agrees very well with ϕ . The angle between the Ru-O(2) bond and the long axis, $\theta\text{-O}(2)$, is smaller than the tilt of the basal planes. The temperature dependence of the tilt angle, see Fig. 6, indicates a tilt transition several hundred degrees Kelvin above room temperature, and, hence, suggests that the group-theoretical distortion sequence indicated in the left part of Fig. 4(a) re-

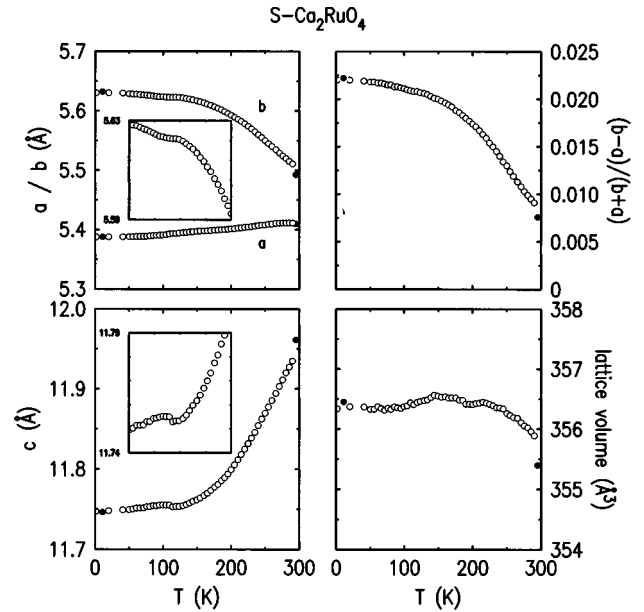


FIG. 3. The lattice constants, orthorhombic strain and lattice volume in S-CRO as a function of temperature. The open circles denote the results obtained on *G4.1* and the filled ones those of *3T.2*. The insets show details of the temperature dependences close to the magnetic ordering; their abscissa agree with those of the main plots.

flects the transition scheme. In general the octahedra in S-CRO are only little distorted. For instance, the orthorhombic distortion follows the rigid tilt: the octahedra tilt nearly around *b* which is the longer lattice parameter. Therefore, the difference in the lengths of the edges of the octahedron basal planes remains small. The rigid character of the RuO_6 octahedron is related to the pronounced covalent character of the Ru-O compounds. The covalent nature of these bonds was also deduced from the analysis of the lattice dynamics in SRO (Ref. 22) and is well explained by the strong Ru-4*d* O-2*p* orbital overlap.

The data obtained with the longer wavelength at *G4.1* are insufficient for a full structure determination. In order to suppress correlations during the fits, the parameters not depending on temperature, Ca-*y*, O(1)-*x,z*, and O(2)-*y*, see the *3T.2* results shown in Table I, were fixed. In addition the thermal parameters were constrained to the values interpolated to the high-resolution data. There is still some correlation between the Ca and O(2) displacements parallel to the planes which limit the significance of the corresponding results. Nevertheless, the good agreement between the *G4.1* results and the high-resolution data at 295 and 11 K demonstrates the reliability of these data. At low temperatures additional magnetic reflections were taken into consideration, see below. Besides these magnetic reflections, no new intensities appear on cooling. Therefore, we conclude that no structural transition occurs in S-CRO below room temperature. Figure 6 shows the temperature dependence of the three tilt and rotation angles characterizing the two distortions and demonstrates the different character of the tilt and rotational deformations.

The in-plane parameters show thermal expansion coefficients of different signs (see Fig. 3); *a* is shortening upon cooling but much less than what would correspond to the

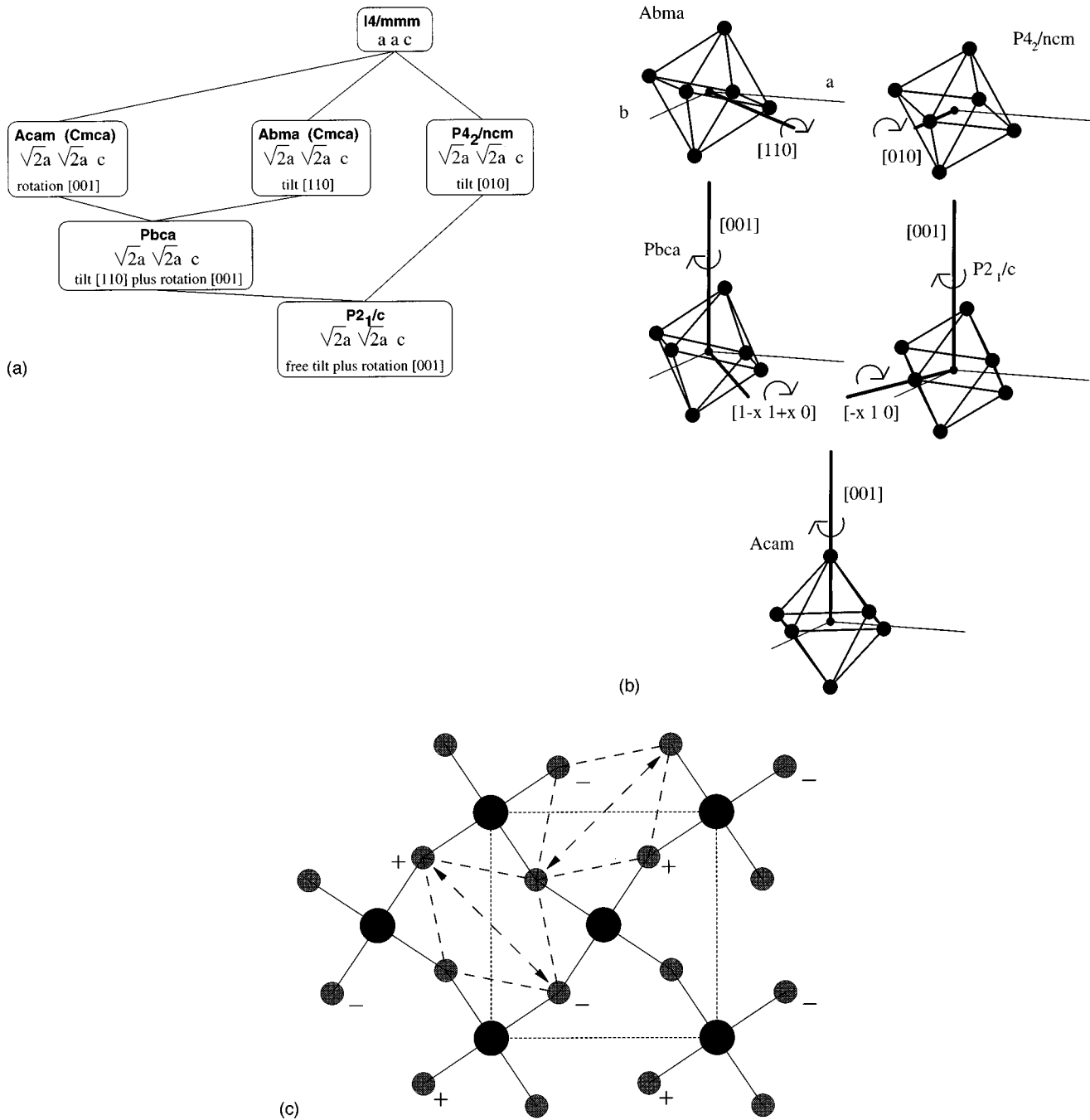


FIG. 4. (a) Schematic picture showing the group-subgroup relations together with the associated distortion types and lattice changes. A line indicates a transition into a subgroup. (b) Rotation and tilt schemes of an ideal rigid octahedron. The thin lines correspond to a and b axes of the $14/mmm$ structure, i.e., they pass through the Ru-O bonds in the nondistorted structure. The thick lines show the rotation or tilt axes, when viewed along these lines towards the Ru all rotations are clockwise. Above left: LTO-type tilt corresponding to space group $Abma$; above right: LTT-type tilt corresponding to $P4_2/nm$ space group; middle left: LTO-tilt plus rotation corresponding to $Pbca$ space group; middle right: LTT-tilt plus rotation corresponding to $P2_1/c$ space group; lower: rotation corresponding to $Acam$ space group. (c) Schematic picture of a single RuO_2 layer distorted by a LTT-tilt combined with a rotation corresponding to space group $P2_1/c$ (the Ru ions are designated by the larger dots). The displacements of the O(1) sites perpendicular to the plane are indicated by plus and minus signs, half of the O(1) sites remain on the layer in the LTT-tilt mode.

rotation of octahedra with temperature-independent size. As the b direction is almost parallel to the tilt axis, the strong, more than 2%, increase of b directly translates into an elongated Ru-O(1) distance. The $Pbca$ symmetry allows a splitting of the two Ru-O(1) bond distances, which, however, remains negligible as it is seen in the high-resolution results in Table II. The $G4.1$ data does not allow to distinguish the

small difference; therefore, we show in Fig. 7 the averaged Ru-O(1) distance as a function of temperature. The strong increase of this bond of about 2% on cooling should be considered as extremely anomalous compared to the usual thermal contraction of some 10^{-3} seen for example in SRO.^{12,23} The elongation of the in-plane bond is accompanied by a shrinking of the Ru-O(2) distance of a similar amount. Due

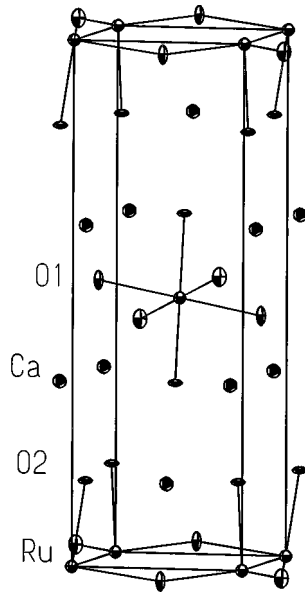


FIG. 5. The low-temperature structure of the $PbcA$ phase of CRO in the form of an Ortep plot. The drawn ellipsoids represent 85% probability density, and the box shows the unit cell of an undistorted tetragonal structure.

to the double weight of the in-plane distance, the average Ru-O bond distance still increases on cooling. The flattening of the RuO_6 octahedron along the c axis might be associated to a Jahn-Teller distortion. Indeed, the temperature depen-

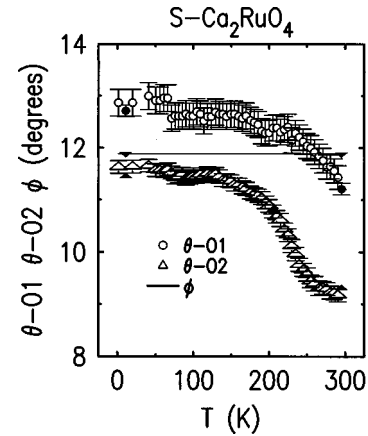


FIG. 6. Tilt [$\theta\text{-O}(1)$ and $\theta\text{-O}(2)$] and rotation angles (ϕ) in S-CRO as a function of temperature. The open symbols denote the results obtained on the high flux diffractometer and the filled symbols those of the high-resolution experiments. Due to the used constraint, ϕ was not determined with the high flux data.

dence of the lattice constants is rather similar to that found in some manganites where it appears ascertained to arise from a Jahn-Teller effect.²⁴

Coming back to the lattice constants given in Fig. 3, one notices a saturation of the increase in b on cooling near 110 K, i.e., the temperature where the magnetic ordering sets in, see below. A similar effect can be seen in both Ru-O bond distances. In addition, the c parameter (long axis) exhibits

TABLE II. Several bond distances and angles obtained from the structural refinements shown in Table I; for comparison, we show also values for Sr_2RuO_4 from Ref. 12.

	S-CRO 295 K $PbcA$	S-CRO 11 K $PbcA$	O-CRO 11 K $PbcA$	O-CRO 295 K $P2_1/c$	Sr_2RuO_4 295 K $I4/mmm$
Ru-O(1) (\AA)	1.986(2) 1.993(2)	2.015(2) 2.018(2)	1.976(4) 2.007(4)	1.915(3)/1.920(4) 1.963(4)/1.953(4)	1.9355
Ru-O(2) (\AA)	1.995(2)	1.972(2)	2.014(4)	2.048(3)/2.048(3)	2.0599
Ru-O _{aver} (\AA)	1.991	2.002	1.999	1.975	1.977
Vol RuO_6 (\AA^3)	10.52	10.69	10.65	10.24	10.28
Ca-O(1) (\AA)	2.298(4) 2.436(4) 2.652(4) 3.230(4)	2.292(3) 2.433(3) 2.565(3) 3.313(3)	2.303(6) 2.425(6) 2.646(6) 3.235(6)	2.298(11)/2.266(16) 2.454(44)/2.492(16) 2.916(14)/2.911(16) 3.088(14)/3.078(15)	2.692
Ca-O(2) (\AA)	2.294(3) 2.380(4) 2.424(4) 3.089(4) 3.109(4)	2.287(3) 2.362(3) 2.399(3) 3.118(3) 3.296(3)	2.258(6) 2.379(6) 2.433(7) 3.093(6) 3.132(7)	2.276(9)/2.264(9) 2.407(12)/2.540(17) 2.558(17)/2.566(20) 2.771(17)/2.772(20) 2.935(12)/2.805(17)	2.439 2.737
Ca-O(1) _{aver} (\AA)	2.654	2.651	2.652	2.688	
Ca-O(2) _{aver} (\AA)	2.659	2.692	2.659	2.589	
Ca-O _{aver} (\AA)	2.657	2.674	2.656	2.633	2.684
Vol. CaO_9 (\AA^3)	39.16	39.21	39.05	38.72	42.58
Ca-bond valence sum	2.006	2.072	2.044	1.929/1.891	
$\theta\text{-O}(1)$ (deg)	11.21(11)	12.72(11)	10.79(11)	5.06(33)	
$\theta\text{-O}(2)$ (deg)	9.31(5)	11.45(5)	9.75(10)	4.50(12)	
ϕ (deg)	11.880(2)	11.881(2)	11.905(3)	13.28(2)	

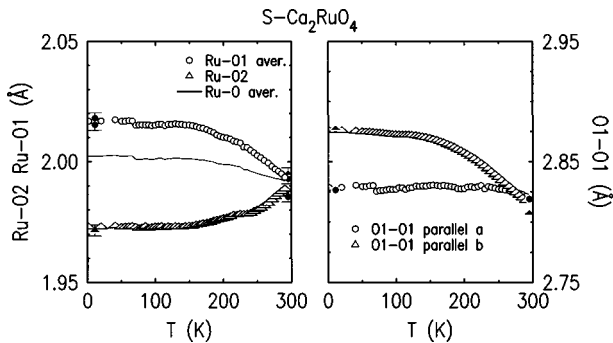


FIG. 7. The Ru-O(2) (apex) and the averaged Ru-O(1)-bond distances (left) and the octahedron basal plane edge lengths along a and b in S-CRO ($Pbca$) as a function of temperature. The open symbols denote the results obtained on the high flux diffractometer and the filled symbols those of the high-resolution experiments.

anomalous behavior near the magnetic ordering. The strong shortening of the long axis upon cooling may partially be explained by the increasing tilt of the octahedron; however, the observed tilt increase is too small for explaining the observed reduction: assuming a constant octahedron length, one obtains only 0.7% shortening which represents only one third of the observed effect. The c -axis shortening is mainly caused by the reduction of the Ru-O(2) bond distance. Below the magnetic transition the c axis exhibits little thermal expansion. A similar observation below the ferromagnetic ordering in metallic SrRuO_3 has been interpreted as an Invar effect.¹⁹

The volume thermal expansion is small when compared to the effects along the axes; however, the increase of volume upon cooling from room temperature to 150 K is rather anomalous; and again there seems to be an influence of the magnetic ordering.

Figure 3 shows the temperature dependence of the orthorhombic strain, $\epsilon = (b-a)/(a+b)$, which at low temperature, is more than twice as high as at room temperature. One may define the tilt angle as the order parameter Q of the phase transition from a hypothetical high-temperature phase towards $Pbca$. For this case, simplest Landau theory²⁵ predicts that the orthorhombic strain is coupled to the order parameter quadratically, $\epsilon \propto Q^2$, which is certainly not fulfilled in S-CRO. Whereas the reduced temperature dependence of the tilt angle indicates a transition at least several hundreds of degree Kelvin higher than room temperature (Fig. 6), the orthorhombic strain extrapolates to zero already near 400 K (Fig. 3). Furthermore, the tilt can explain only half of the orthorhombic strain; the other part results from different octahedron basal plane edges parallel to a and parallel to b , see Fig. 6. The pronounced increase of the edge length along b clearly demonstrates that the orthorhombic strain is not directly coupled to the tilt angle. Like the temperature dependence of the RuO-bond distances, this behavior may be explained by a Jahn-Teller-like coupling varying with temperature in the $Pbca$ -distorted phase.

The most pronounced differences when compared to an undistorted K_2NiF_4 structure are found for the Ca-O distances, see Table II. In the undistorted structure there is only one Ca-O(1) bond distance, which is split into four different values in S-CRO, the ratio between longest and shortest Ca-O(1) distances approaches a factor of 1.4. Concerning the

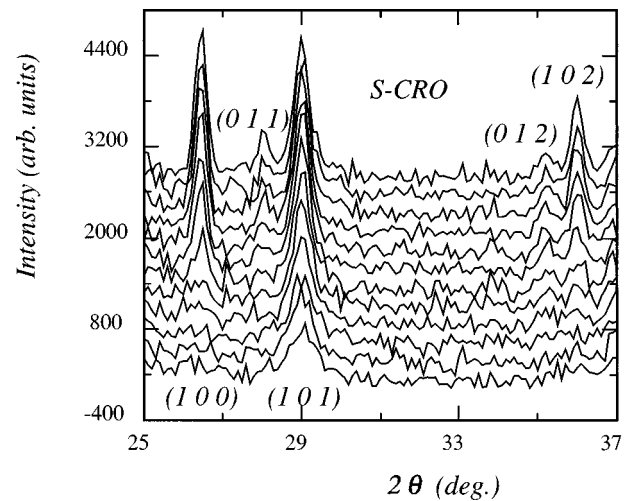


FIG. 8. Part of the high flux diffraction pattern for different temperatures showing five magnetic reflections in S-CRO. The patterns are shifted vertically for clarity, the highest line corresponds to 80 K and the difference between two lines to approximately 5 K.

bonds with the O(2) sites, the ideal structure possesses two distinct types, an unique one parallel to the long axis and four equivalent bonds almost perpendicular to the long axis. The latter four distances are as strongly modified as the Ca-O(1) distances. These strong effects indicate that the Ca-O bonds are important for the mechanism of the tilt and rotation transitions in S-CRO, similar to the observations in Sr-doped La_2CuO_4 .²⁶

B. Magnetic structure in the S-CRO

Figure 8 shows a part of the high flux patterns obtained at different temperatures between 20 and 150 K. On cooling there are additional reflections appearing, which can be indexed in the $Pbca$ lattice with odd h or k . Therefore, these peaks correspond to a superstructure in comparison to the undistorted K_2NiF_4 lattice and to an antiferromagnetic ordering. However, the distinct new reflections do not show the same temperature dependence indicating two coexisting magnetic modes. The ordered moments corresponding to the two modes described below were refined together with the structural model and are shown in the upper part of Fig. 9. One type, for example (1 0 1) starts to increase already near 150 K and saturates near 110 K when a second type of magnetic reflections [(1 0 0) and (0 1 1)] starts to grow; the latter reflections saturate at much lower temperature. For comparison we show in the lower part of Fig. 9 the magnetic susceptibility of the same sample; there is excellent agreement between the anomalies observed there and the characteristic temperatures for the magnetic intensities observed in the neutron diffraction.

Unfortunately there is already some broadened intensity near the position of the (1 0 1) peak at higher temperatures; the maximum of the additional peak corresponds to about 2.5% of the strongest intensity. The (1 0 1) reflection is forbidden in $Pbca$ symmetry; furthermore, it cannot be explained by an experimental artifact, as for instance O-CRO measured under the same conditions does not show this intensity. Several attempts were undertaken in order to explain this feature by a reduced structural symmetry, but the most

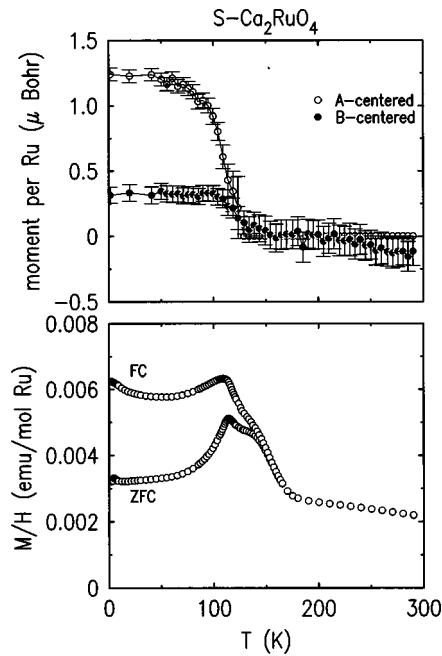


FIG. 9. Results of the magnetic refinements for S-CRO: the filled circles show the ordered moment corresponding to the *B*-centered magnetic mode and the open circles the moment corresponding to the *A*-centered mode (scaled to 100% volume fraction). The lower part shows for comparison the magnetic susceptibility at 1 T measured on a part of the sample.

probable models did not yield a significant structure factor for that reflection. The broadening may indicate some local distortion for example of the rotational scheme, which was already assumed for Sr_2IrO_4 .¹⁰ That the magnetic ordering of the Ru spins would persist up to high temperature appears rather unlikely due to the low Néel temperatures commonly observed in ruthenates. For the analysis of the magnetic data the contribution of this spurious peak was subtracted from the fitted intensity.

The two different types of peaks cannot correspond to a magnetic structure with one propagation vector. Assuming an antiferromagnetic ordering in one plane, the only possibilities to arrange neighboring planes are in an *A*- or in a *B*-centered way as depicted in Fig. 10. This means that either the Ru at (0 0.5 0.5) or the one at (0.5 0 0.5) is equivalent to the one at (0 0 0). It is evident that the first type of reflections (101) corresponds to the “*B*-centered” arrangement and the second type [(100) and (011)] to the “*A*-centered” one. Further inspection of the intensities of the different reflections within one family leads to the conclusion that for both types the ordered moment is aligned along *b*, and hence parallel to the elongation of the octahedron basal plane. The two observed antiferromagnetic arrangements depicted in Fig. 10, correspond exactly to the La_2CuO_4 and La_2NiO_4 types of ordering, which were described for example in Ref. 27. Below 150 K the ordered moments according to these two magnetic modes were refined together with the structural model. The obtained values are presented in Fig. 9. It appears unlikely that the magnetic structure is single phase but that complicated. It appears more reasonable to assume that there is a phase separation into two coexisting phases. A similar coexistence of these two magnetic modes was already re-

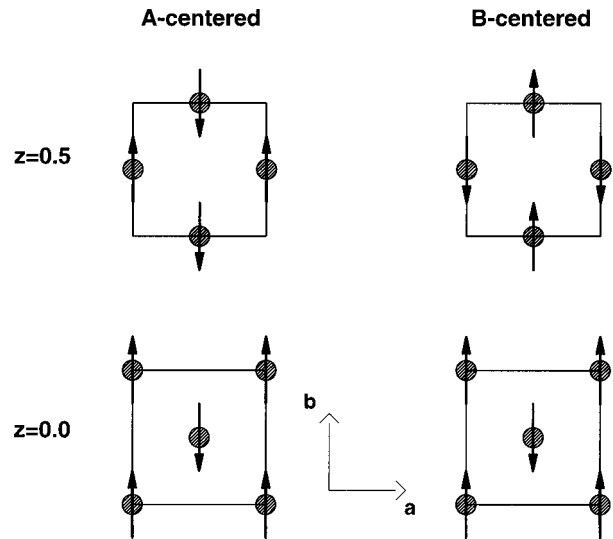


FIG. 10. Schematic picture of the two magnetic modes in space group *Pbca*. Only the spin directions of the Ru’s at $z=0.0$ and $z=0.5$ are shown. The propagation vector of the *A*-centered mode is (1 0 0) (La_2CuO_4 type) and that of the *B*-centered type is (0 1 0) (La_2NiO_4 type).

ported for Pr_2NiO_4 (Ref. 28) and $(\text{La}/\text{Nd})_2\text{CuO}_4$.²⁷ It is, furthermore, astonishing that the ordered moment of the first phase saturates just when ordering corresponding to the second mode sets in. The *A*-centered mode can be considered as the main contribution to the antiferromagnetic ordering. The implication of the antiferromagnetic arrangement for the observation of the weak ferromagnetism will be discussed together with the results for O-CRO.

In order to estimate the ordered moment one has to sum over the two phases yielding a value of $1.3\mu_B$ smaller than $2\mu_B$ expected for Ru^{4+} . One further should take into account that we have used the form factor for Ru^{1+} given in the International Tables for Crystallography²⁹ for calculating the magnetic intensities, which, at higher *Q* values, overestimates the real form factor of the strongly hybridized arrangement in CRO. Therefore, the corrected ordered moment should be somewhat higher, approaching the ideal value.

The magnetic order influences the crystal structure as can be seen in the anomalies of the lattice parameters near T_N , see Fig. 3. A possible effect for the tilt angle shown in Fig. 6 is difficult to separate from the expected low-temperature saturation. In contrast, there is evidence that the temperature dependence of the RuO_6 octahedron distortion changes near the magnetic transition, see Fig. 7. The antiferromagnetic ordering should be dominated by the in plane superexchange constant between neighboring Ru’s, which will sensitively depend on both bond lengths and bond angles. Concerning the bond angle, maximum interaction is expected for flat and undistorted RuO_2 planes, corresponding to a bond angle of $\phi\text{-Ru-O(1)-Ru}=180^\circ$. The strong distortion, $\phi\text{-Ru-O(1)-Ru}\sim 151^\circ$ in S-CRO at 11 K, weakens the antiferromagnetic contribution.³⁰ However, the same distortion should also significantly alter the ferromagnetic interaction. A quantitative analysis of the magnetic order in CRO will require *ab initio* calculations. The deformation of the octahedron which might be associated with the Jahn-Teller effect, is obviously coupled to the in-plane and interplane cou-

pling. Also the elongation of the octahedron basal plane along b appears closely coupled to the magnetism, since the ordered moment follows this elongation.

C. Crystal structure of O-CRO

Room temperature structure of O-CRO. The high-resolution pattern obtained with O-CRO at room temperature has little resemblance to that of S-CRO, see Fig. 1, suggesting a rather different structure, as already deduced from the much larger c axis (long- c phase). However, the huge temperature dependences of the structure of S-CRO have shown that in this system essential distortions may occur without changing the fundamental structure of CRO.

First refinements indicate that O-CRO possesses a structure derived from the K_2NiF_4 type with a quite peculiar distortion scheme but without any doubling of the long axis. We checked the rotational distortion found in Gd_2CuO_4 ,¹⁴ space group $Acam$. This refinement yields a better agreement though it still remains rather imperfect. The superlattice peaks which are of type $(2\ 1\ l)$ or $(1\ 2\ l)$ are well described; however between two neighboring reflections of that type some broad intensity exists, which may point to an imperfection in the stacking of the rotational distortion. A similar observation was reported also for Sr_2IrO_4 .¹⁰ Some undescribed intensities indicate that in addition to the rotational distortion a long range tilt deformation exists in the O-CRO phase too. However, the quasitetrragonality of the lattice, which prevents a detailed analysis of extinction rules, suggests a space group other than $Pbca$. Nevertheless, a satisfying description can be obtained in the latter model.

The rotational distortion described in space group $Acam$ does not induce a strong orthorhombic splitting though it is allowed by symmetry. In this case, the orthorhombicity is only caused by the stacking of the distorted planes—a single layer still has a fourfold axis.^{14,31} In contrast, the tilt distortion may easily induce orthorhombicity. We assume that the distinct structure in O-CRO is due to a different tilt scheme. Because of the quasitetragonal structure a tilt scheme corresponding to the LTT structure of the cuprates should presumably be involved. Therefore, we looked for the subgroups of the LTT space group $P4_2/ncm$. Since the rotation should not induce a lattice larger than that of the LTT structure (see above) the mode involved in such a transition has to be an even Γ mode. Among the few candidates listed in Ref. 17, only $P2_1/c$ allows the desired distortion. In $P2_1/c$, there are two O(1) sites within one plane as it is necessary in a LTT tilt scheme: in the ideal case, only one site is moving perpendicular to the planes. However, in $P2_1/c$, also the Ca, Ru, and O(2) sites are split which considerably increases the number of free parameters in this structure. $P2_1/c$ is also a subgroup of $Pbca$ (see Fig. 4): a symmetry relation of $Pbca$ which is nonexistent in $P2_1/c$ is

$$(0.5-x\ 0.5+y\ z). \quad (1)$$

The distortion of a single RuO_2 layer is shown in Fig. 4(c).

First refinements with the full number of free parameters indicate that only the O(1) and the Ca site violate the symmetry operator (1); therefore the number of free parameters was reduced by constraining most of the sites according to Eq. (1). Furthermore, it turned out that only one of the O(1)

sites has a nonzero z position as in an ideal LTT structure. Therefore, the description in $P2_1/c$ needs only three additional parameters: $\text{Ca}'\text{-}x$, $\text{Ca}'\text{-}y$ and the monoclinic angle β , which, however, remains close to 90° . In addition it was necessary to refine the amount of the CaRuO_3 impurity phase, which possesses a larger volume ratio than in S-CRO. The final structural parameters are presented in Table I. The refinement of the $P2_1/c$ model gives a slightly better description than the one according to $Pbca$; the strongest deviation arises from the O(1) split. It was checked that this behavior can be excluded for S-CRO, where refining the two O(1) sites within $P2_1/c$ symmetry yields shifts along the long axis which are identical within their errors. The temperature-dependent studies show, that the O-CRO phase remains quasitetragonal upon cooling down to 160 K, in contrast to the strongly varying orthorhombic strain of the $Pbca$ phase in S-CRO, where it possibly passes zero above room temperature. This discrepancy in the temperature dependence supports the distinct symmetry in both phases. However, it may not be excluded that the $P2_1/c$ symmetry in O-CRO results from averaging short-range orthorhombic distortions similar to the structure of S-CRO (see below). The definite analysis of the space group in O-CRO requires certainly single-crystal diffraction.

The refinement in the $P2_1/c$ is still less satisfying than those of the S-CRO data sets, especially the high flux data indicate some weak but unexplained reflections (note, that the CaRuO_3 impurity phase has been taken into consideration during the refinements). These peaks cannot be indexed even when doubling all parameters of the $P2_1/c$ structure, which would already require a rather complicated distortion pattern. Furthermore, they do not show the same and very characteristic temperature dependence of the main reflections, see below. Attempts to describe them by the starting materials CaCO_3 and RuO_2 were unsuccessful. These peaks might be due to a multilayer Ruddlesden-Popper phase.³²

The characteristic bond lengths and angles of O-CRO are given in Table II. The main distortion elements are rather different when compared to the results on S-CRO. Whereas the rotational angle is slightly larger in O-CRO, the tilt is strongly suppressed. The long- c phase appears less favorable for a large tilt than the LTO-like $Pbca$ phase, an effect which is compensated by the increased rotation. However, while explaining the distinct symmetries, these differences appear not to be the most important features. Already the lattice volume, which is about 1.5% smaller in the $P2_1/c$ phase, indicates essential changes in the bond lengths too. These effects are most pronounced for the Ru-O distances, which show a small octahedron flattening in the $Pbca$ phase in S-CRO. In the long- c phase in O-CRO, there is a strong elongation of the octahedra along the long axis, which together with the reduced tilt angle accounts for the larger long axis. The symmetry in O-CRO appears to impose important constraints on the Ru octahedra which appear to be relaxed in the $Pbca$ structure. The in-plane Ru-O distance is the structural parameter most important for the electronic properties, this distance is about 2.5% smaller in O-CRO. It seems interesting to note, that the RuO coordination in O-CRO which is metallic at room temperature, is rather similar to the one in metallic Sr_2RuO_4 .

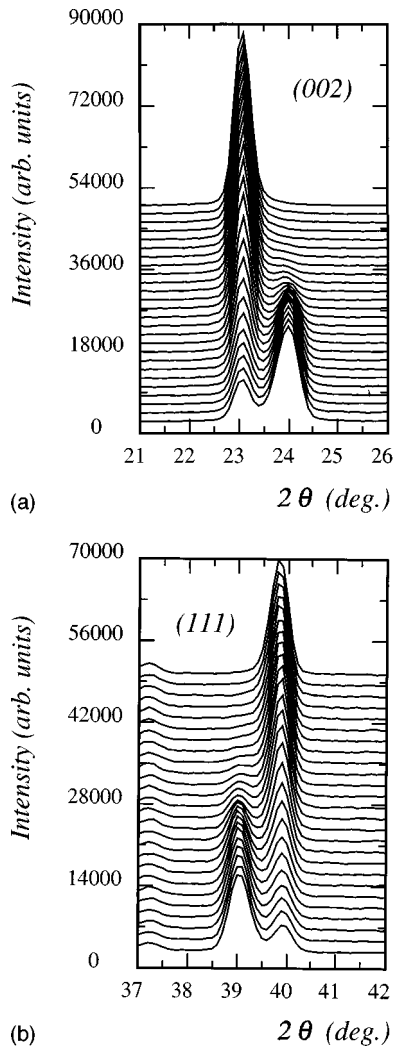


FIG. 11. Parts of the diffraction patterns obtained with G4.1 on O-CRO showing the (002) (a) and (111) reflections (b) at different temperatures. The profiles are shifted vertically with the lowest line showing the data obtained at 1.5 K. The successive lines correspond to temperatures of 20, 40, and then to ~ 5 K temperature steps.

The average RuO bond distance is about 1% smaller in the long- c phase. Hence, the increased lattice volume in S-CRO is mainly due to the Ru coordination (see Table II). The differences in the Ca-O bonds are less dramatic: the CaO-coordination polyhedron appears more regular in the long- c phase.

Low-temperature phase transition and structure. Figure 11 shows parts of the diffraction patterns obtained using the high-flux diffractometer upon heating; these figures show the profile shapes of the (0 0 2) and (1 1 1) reflections in $Pbca$ notation. The essential changes manifest a structural rearrangement related to a first-order phase transition. The reflections corresponding to the room-temperature phase depend only slightly on temperature concerning their positions but their intensity is continuously transferred to the new peaks at low temperatures. The position of the new peaks indicate that the low-temperature O-CRO phase exhibits a smaller long axis and larger in-plane parameters, as does the $Pbca$ phase of the S-CRO and, indeed, it turned out that the new phase can be described in the $Pbca$ structure. The 11 K pattern measured on the high-resolution diffractometer could

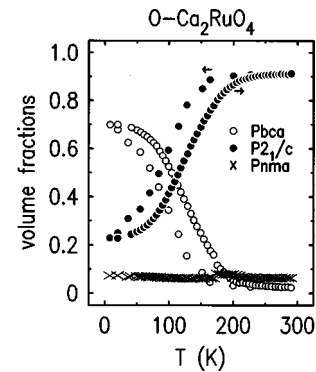


FIG. 12. Partial volume fractions of the three structural phases in O-CRO as a function of temperature, the Pnma phase corresponds to the CaRuO_3 perovskite. The arrows indicate the temperature variation.

be well described by a superposition of three phases: the $P2_1/c$ O-CRO structure, the $Pbca$ phase like in S-CRO and the perovskite CaRuO_3 impurity phase. A similar superposition was then used to describe the high flux data at intermediate temperatures. The latter data allowed us to determine the temperature-dependent volume ratios of the different phases in this sample which are depicted in Fig. 12. The perovskite volume ratio is constant, as expected for an impurity phase. At 200 K the transition towards the $Pbca$ phase sets in, which remains incomplete even at the lowest temperatures: 24% of the sample remain in the long- c structure. There is a pronounced hysteresis of about 40 K between cooling and heating which confirms the first-order nature of the transition.

The results of the 11 K high-resolution structure analysis are presented in Tables I and II. The structure is very similar to that of S-CRO at the same temperature which is characterized by a shorter c axis (short- c phase). It should be noted that the rotational angle ϕ , which was significantly enhanced in the $P2_1/c$ structure, is shifted to exactly the same value as in S-CRO where it was found to be temperature independent, see Table II. The angles characterizing the tilt of the octahedra are strongly increased when compared to the $P2_1/c$ room-temperature values but are still lower than those of S-CRO at low temperature. The latter tendency is also followed by the orthorhombic strain. As discussed above, the strong deformation of the RuO_6 octahedron in the long- c phase constitutes an essential structural difference between the two room-temperature structures. This deformation is also relaxed by the first-order transition on cooling. The octahedron in the $Pbca$ structure in O-CRO at 11 K is more regular than that of S-CRO. The inequivalent Ru-O bonds have almost the same distance and also the edge lengths of the octahedron basal planes are more similar. The latter splitting is related to the smaller orthorhombic strain in the $Pbca$ structure. In order to briefly resume the low-temperature structure of the O-CRO, one may note that it corresponds to the $Pbca$ structure of S-CRO with all characteristic distortions being less pronounced.

Figure 13 shows the lattice parameters for the two phases in O-CRO as a function of temperature. One notices that these parameters also show some hysteretic behavior. On cooling the $Pbca$ parts of the sample show stronger orthorhombic strain and a smaller long axis—both effects indicate a character closer to the one in S-CRO. The parts transform-

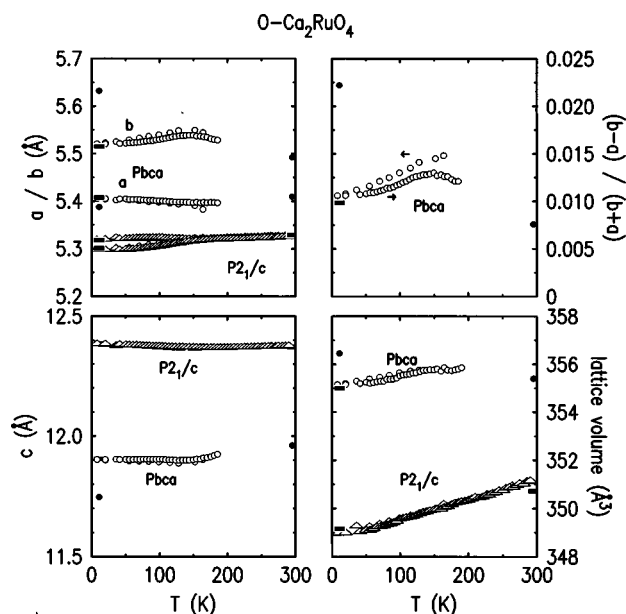


FIG. 13. The lattice constants, orthorhombic strain and lattice volume in O-CRO as a function of temperature. The open circles denote the results obtained on G4.1 for the $Pbca$ phase and the open triangles those for the $P2_1/c$ long- c phase. The filled rectangles show the corresponding high-resolution results; furthermore, the lattice constants of S-CRO are shown for comparison indicated by the filled circles.

ing on cooling at lower temperature seem to readjust the averaged $Pbca$ structure in O-CRO. The same behavior is also seen in the temperature dependence of the $Pbca$ tilt angle $\theta\text{-O}(1)$. Only little can be learned about the temperature dependence of the long- c phase in O-CRO because of the structural transition of the major part of the volume. The $P2_1/c$ lattice parameters exhibit much smaller temperature dependences than those of the $Pbca$ phase, for example the long axis varies within a relative change of 2×10^{-3} which may be considered as a normal value for a compound with pronounced covalent bonding. Also the volume shows a normal thermal expansion. Below 200 K, when the transformation starts, the long axis begins to increase and a more pronounced orthorhombic splitting is observed; the monoclinic angle is always close to 90° . Like in the $Pbca$ parts, the phase separation may also allow the long- c parts of the sample to relax. The long- c structure is far too complicated for being determined as a minority phase: even the high-resolution data allowed us only to refine Ca-z , $\text{O}(2)\text{-z}$, and $\text{O}(1)\text{-z}$ at 11 K. The first two parameters show no effect and the last one indicates a slight increase of the tilt angle in the long- c phase upon cooling, which is supported by the high flux data.

Mechanism of the short- c -long- c transition. The mechanism of rotational and/or tilt transitions in perovskite-related compounds is well analyzed in several families of type $A_1\text{BO}_3$.^{33,34} A high symmetry imposes strong constraints for the coordination polyhedra around the A and B cations. This can be easily seen in the cubic perovskite structure, which imposes that the $A\text{-O}$ distance corresponds to exactly $\sqrt{2}$ times the $B\text{-O}$ distance. Analyzing the empirical ionic radii one may estimate whether the cubic perovskite would be stable for the atoms A , B , and O or not.³³ For the more

complex structure types like K_2NiF_4 the analysis becomes more complicated due to the degrees of freedom which permit the system to reduce the internal misfit. In these cases it appears more convenient to analyze the stability of the structure using the bond valence sum analyses³⁵ when available. Such an analysis is perfectly adapted to describe the phase transition in the La_2CuO_4 family.²⁶ For Ru the necessary parameters are not yet determined; therefore, one has to restrict this analysis to the Ca site. The analysis of the Sr_2RuO_4 compound yielded a perfect stability of the ideal structure,¹² using the same structure with Ca bond valence parameters yields a bond valence sum of 1.29 clearly indicating the instability induced by the Ca ion. The smaller Ca needs a smaller polyhedron, therefore, it exerts a higher pressure on the RuO bonds. In the $I4/mmm$ symmetry it is impossible to reduce the CaO polyhedron volume without simultaneously increasing the pressure on the Ru-O bonds. In order to re-equilibrate the internal pressure it is favorable to lower the symmetry and then reduce the Ca-O distances separately via the new degrees of freedom. The bond valence sums of Ca in S-CRO and O-CRO at room temperature, given in Table II, indicate an almost equilibrated structure for both compounds. From this point of view it appears impossible to explain the short- c -long- c transition.

The role of the oxygen content is to further tune the structural balance.³⁴ Additional oxygen will relax the pressure implied by the misfit, since it oversaturates the Ca coordination and a charge transfer towards the RuO_2 planes results in smaller Ru-O equilibrium distances. The latter requires an oxidation of Ru higher than $4+$ which is also found in the double perovskite Sr_2RuYO_6 .⁷ From the phase diagrams of $\text{La}_2\text{CuO}_{4+\delta}$ (Ref. 36) and $\text{La}_2\text{NiO}_{4+\delta}$ (Ref. 37) it is well known that even small amounts of interstitial oxygen which are undetectable with the powder neutron-diffraction technique, significantly shift the structural transitions. We suggest a similar behavior for the CRO compounds. The highly distorted CRO structure is certainly favorable for an insertion of additional oxygen during the annealing at 400°C , which reduces the structural distortion as, indeed, the comparison between the $Pbca$ structures in the two samples at low temperature confirms. Thermogravimetric analysis (TGA) studies on the two samples allow to determine the enhanced oxygen content in O-CRO, $\delta=0.07(1)$ corresponding to the formula $\text{Ca}_2\text{RuO}_{4+\delta}$, whereas we find $\delta=-0.01(1)$ in S-CRO.

Another impact of the interstitial oxygen consists in the introduction of sizeable disorder, since around an excess oxygen the tilt distortion should become considerably reduced. A similar disorder was discussed in the context of the LTT-tilt structure in $\text{La}_{2-x-y}\text{Sr}_x\text{R}_y\text{CuO}_4$ with R being a rare earth,³⁸ the LTT-tilt scheme appears more favorable in order to adapt variations in the ionic radii of the atoms occupying the La site than the LTO scheme.³⁹ This statement is supported by the fact that the transition temperature from LTO to LTT in these compounds depends on the variation of the ionic radius rather than on its average value.³⁹ Note, that the LTT phase can be induced by smaller ions [R 's substituted into $\text{La}_{2-x}\text{Sr}_x\text{CuO}_4$ (Ref. 38)] as well as by the substitution of larger ions [$\text{La}_{2-x}\text{Ba}_x\text{CuO}_4$ (Ref. 16)]. That disorder is important for the stabilization of the $P2_1/c$ structure is further supported by the observation of this structure in a

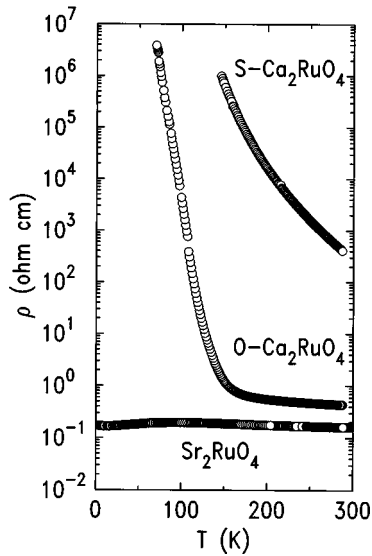


FIG. 14. Resistivity of the two $\text{Ca}_2\text{RuO}_{4+\delta}$ -samples studied in this work compared to the resistivity of SRO. In contrast with the insulating behavior of S-CRO, a metal-insulator transition occurs below about 160 K in O-CRO.

sample prepared at high temperature,⁸ which exhibits oxygen vacancies according to recent TGA studies.⁴⁰ Taking this disorder into account, one may even not exclude that the $P2_1/c$ symmetry results from averaging locally orthorhombic domains. Determining the real structure of the small tilt distortion in O-CRO requires further diffraction studies on single crystals,—which, however, might be difficult to obtain—or measurements using local probes. Cao *et al.* report that their single crystals do not support any O treatment;⁹ assuming that the oxygen content drives the first-order transition one may understand that attempts to vary it in a single crystal will destroy the crystal.

The subtle hysteretic effects in the $Pbca$ structure should be interpreted by small O-phase segregation involved in the short- c –long- c transition. However, several arguments render very unlikely that such a mechanism drives the transition. First, the observation of the long- c phase is not only restricted to oxygen-rich samples, it was also observed in deficient and Sr-substituted samples.^{8,40} Second, the inclusion of additional oxygen raises the symmetry in $\text{La}_2\text{CuO}_{4+\delta}$ (Ref. 41) and in $\text{La}_2\text{NiO}_{4+\delta}$ (Ref. 42) from $Abma$ to $Fmmm$. In analogy the space group of O-CRO with additional oxygen destroying the tilt long-range order should be $Acam$ with split oxygen positions; the corresponding refinements, however, cannot describe the data as well as $Pbca$ or $P2_1/c$, i.e., there is a long-range tilt in O-CRO. Third, a dominant segregation of the excess oxygen towards the $P2_1/c$ phase, where the amount of excess oxygen would be a factor close to four larger, should decrease the tilt angle, which, however, is found to increase on cooling. And fourth, the largest structural effect at the short- c –long- c transition, the increase of the in-plane RuO-bond distance by 2.5%, has no analog in nickelates or cuprates.^{36,37,41,42}

Figure 14 shows the temperature dependences of the resistivity in both CRO compounds. Whereas S-CRO exhibits insulating behavior in the entire temperature range, O-CRO shows a crossover from constant resistivity or metallic be-

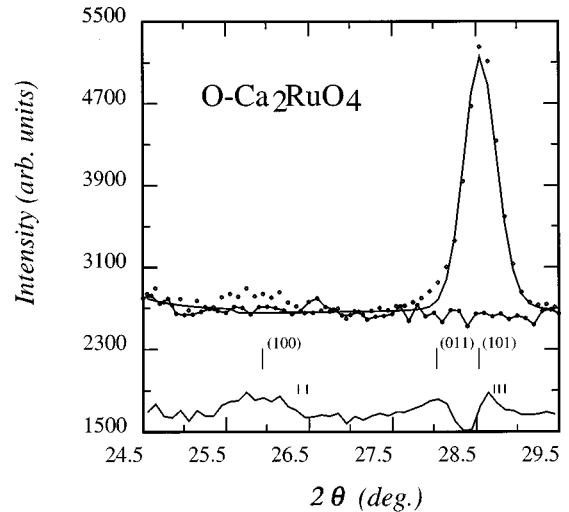


FIG. 15. Part of the diffraction pattern obtained with G4.1 on O-CRO at 1.5 K (circles) and 290 K (connected circles). The line shows the calculated profiles taking into account the $P2_1/c$ structure, the $Pbca$ structure, the B -centered magnetic mode and the CaRuO_3 impurity phase. The long vertical bars indicate the positions of the magnetic reflections in the $Pbca$ lattice: the (101) reflection corresponding to the B -centered mode clearly exists, while those corresponding to the A -centered mode [(100) and (011)] show only weak diffuse scattering. The smaller bars indicate the positions of magnetic reflections in the $P2_1/c$ lattice.

havior to insulating behavior below about 150 K. Since the resistivity has been measured on cooling, the onset of insulating behavior agrees very well with the onset of the first-order transition into the $Pbca$ phase. One should, therefore, interpret the mixed electronic-structural transition as a metal insulator transition.⁴³ The nonobservation of a similar effect in the resistivity of $\text{La}_2\text{CuO}_{4+\delta}$ at the phase separation⁴⁴ confirms the distinct character of these transitions. The short- c –long- c transition should be compared to metal-insulator transitions in RNiO_3 , where the structural transition is very subtle,⁴⁵ or in some vanadates, where the transition is associated with magnetic order.⁴⁶

D. Magnetic structure of of O-CRO

Figure 15 shows a part of the 1.5 K diffraction pattern obtained with O-CRO on G4.1 together with its description via the Rietveld method and an experimental profile at higher temperature. The comparison of the two temperatures evidences the appearance of the new peaks of magnetic origin. At first sight the magnetic structure seems to be less complicated in the O-CRO compound, as only the B -centered ordering type is dominantly present. The bars indicating the positions of possible Bragg reflections give further evidence that the magnetic phase corresponds to the $Pbca$ lattice indicated by the row of longer bars, (no nuclear $Pbca$ reflection lies within the shown part of the pattern). The (1 0 1) position clearly indexes the magnetic peak, in addition weaker and broadened intensities exist around (1 0 0) and (0 1 1). The positions of the possible magnetic reflections according to the long- c minority phase lattice are given in the last row, they do not correspond to a magnetic intensity, which excludes a comparable antiferromagnetic ordering for the long-

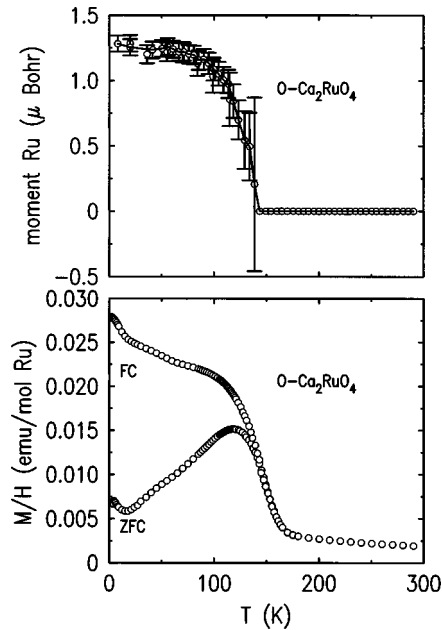


FIG. 16. Results of the magnetic refinements for O-CRO showing the ordered moment corresponding to the B -centered magnetic mode. The lower part shows for comparison the magnetic susceptibility at 1 T measured on a part of the sample (on heating).

c parts of this sample. In contrast to S-CRO one finds an inverted phase volume ratio in the $Pbca$ structure parts of O-CRO: the B -centered structure which is the minority phase in S-CRO is dominant now, and the former main phase is strongly reduced to some short-range-ordered domains.

The appearance of the magnetic peaks agrees with the temperature dependence of the magnetic susceptibility, see Fig. 16. In contrast to S-CRO, the transition is not split in the susceptibility data, which reflects the rather small volume of the second magnetic phase in O-CRO. One should stress that the magnetic moment shown in Fig. 16 is normalized with the scale factor of the $Pbca$ phase, and, therefore, should not experience the strong hysteresis of the structural transition. That this is really fulfilled strongly confirms that the magnetic scattering is due to the $Pbca$ structure only. The diffraction experiment alone cannot rule out that these long- c parts might exhibit ferromagnetic order; however, such a behavior should have become evident in the susceptibility.

As the contribution from the A -centered mode is almost negligible, the summed ordered moment in the O-CRO compound is significantly lower than that of the S-CRO compound.

Due to the strong lattice deformations in the CRO structure the antiferromagnetic ordering induces the appearance of weak ferromagnetism for both types of magnetic order via Dzyaloshinski-Moriya interactions. In this sense the rotation of the octahedra around the long axis is more effective than the tilting around an axis almost parallel to b since the spins are oriented along b . Considering only the rotation one yields a weak ferromagnetic moment along a in a single layer which is ferromagnetically coupled for the B -centered mode and antiferromagnetic for the A -centered mode. This nicely agrees to observations of the magnetic susceptibility, as O-CRO possessing dominantly the B -centered order exhibits the stronger ferromagnetic components, see Figs. 9 and 16.

In O-CRO it is difficult to analyze small structural changes near T_N due to the strong first-order transition occurring in this temperature region. However, magnetoelastic coupling is evidenced by the occurrence of the magnetic order only in the $Pbca$ phase. The nonexistence of magnetic order in the long- c phase can be compared to the magnetism in the cubic Ru perovskites. Whereas SrRuO_3 orders ferromagnetically near 160 K,⁴⁷ CaRuO_3 remains paramagnetic till the lowest temperatures.⁴⁸ It was argued that the by a factor of two enhanced structural distortion in CaRuO_3 reduces the ferromagnetic interaction in comparison to SrRuO_3 .⁵ In analogy to the perovskites the smaller tilt distortion in the long- c phase may favor a ferromagnetic interaction and hence act against the antiferromagnetic order. The influence of the shorter Ru-O distance most probably responsible for the metallic character of O-CRO should even be stronger.

IV. CONCLUSION

The structural studies on the two CRO materials show extreme distortions in comparison to an ideal K_2NiF_4 structure, which are naturally explained by the small ionic radius of Ca^{2+} compared to the Sr_2RuO_4 analog. The rotation of the octahedra around the long axis is almost temperature independent, which indicates that a related phase transition may occur only at elevated temperature if at all. In agreement with our recent phonon-dispersion analysis on SRO,¹³ we conjecture that the rotation represents the intrinsic instability of the 214 ruthenates. In addition to the rotational distortion, both compounds exhibit a tilt distortion which varies below room temperature. At room temperature, the S-CRO compound shows a tilt scheme corresponding to the LTO structure in the cuprates, whereas that of O-CRO resembles the scheme in the LTT cuprate phases with a significantly reduced tilt angle. The latter structure is further characterized by smaller RuO_6 octahedra comparable to metallic SRO. O-CRO exhibits a first-order structural phase transition on cooling, which reaches—at least for the main part of the sample—the same structure as the S-CRO material at low temperature. This transition is characterized by a strong increase of the tilt angle and a strong elongation of the in-plane Ru-O bonds. Furthermore, it is accompanied by a change from metallic to insulating behavior in the electric resistivity.

The variation of the oxygen content induces the significant structural changes. The strong misfit between the Ca and Ru ionic sizes, which drives the enormous structural deformation in both compounds, will strongly favor the insertion of interstitial oxygen like in $\text{La}_2\text{CuO}_{4+\delta}$ (Ref. 36) or $\text{La}_2\text{NiO}_{4+\delta}$.³⁷ In these compounds a small amount of interstitial oxygen can change the structural phase transitions drastically. The disorder induced by nonstoichiometry might favor a LTT-like tilt pattern or reduce the long-range tilt order. Such disorder could lead to a partially coherent superposition of orthorhombic domains in the diffraction experiment and, hence, may be indistinguishable from a real $P2_1/c$ structural model used for describing the data. Further studies are needed to clarify the real structure of the tilt distortion in O-CRO. A partial phase separation may be associated with the first-order transition in O-CRO; however, it cannot explain the transition itself, as it may be related only

to the tilt distortion. The large increase of the in-plane RuO distances is *not* observed, either in the cuprates or in the nickelates; it clearly indicates that this transition should be interpreted as a metal-insulator transition.

The magnetic structure of both compounds is found to be antiferromagnetic similar to the cuprates and nickelates. There are two competing arrangements, one *A*-centered of the La₂CuO₄ type and one *B*-centered of the La₂NiO₄ type, which coexist in the samples. The strongly distorted S-CRO material exhibits a major *A*-centered mode; in contrast, in the *Pbca* phase in O-CRO the *B*-centered mode is dominating, while the other contribution is almost negligible. Strong magnetoelectric coupling is manifested in these compounds by several structural anomalies observed near the Néel temperature in single phase S-CRO. In addition, the nonexist-

ence of magnetic order in the long-*c* phase of O-CRO and the strong dependence of the magnetic structure on subtle structural changes underlines the close coupling. The implication of the antiferromagnetic order, which is not required to occur exactly at the metal-insulator transition, still needs to be clarified.

ACKNOWLEDGMENTS

We are grateful to T. Fujita for helpful discussions. This work has been supported by a Grant-In-Aid for the International Scientific Program: Joint Research from the Ministry of Education, Science, Culture and Sports of Japan, and by CREST (Core Research for Evolutionary Science and Technology) of the Japan Science and Technology Corporation.

- ¹Y. Maeno, H. Hashimoto, K. Yoshida, S. Nishizaki, T. Fujita, J. G. Bednorz, and F. Lichtenberg, *Nature (London)* **372**, 532 (1994).
- ²A. P. Mackenzie, S. R. Julian, A. J. Diver, G. J. McMullan, M. P. Ray, G. G. Lonzarich, Y. Maeno, S. Nishizaki, and T. Fujita, *Phys. Rev. Lett.* **76**, 3786 (1996).
- ³Y. Maeno, K. Yoshida, H. Hashimoto, S. Nishizaki, S. Ikeada, M. Nohara, T. Fujita, A. P. Mackenzie, N. E. Hussey, J. G. Bednorz, and F. Lichtenberg, *J. Phys. Soc. Jpn.* **66**, 1405 (1997).
- ⁴I. I. Mazin and D. J. Singh, *Phys. Rev. Lett.* **79**, 733 (1997).
- ⁵I. I. Mazin and D. J. Singh, *Phys. Rev. B* **56**, 2556 (1997).
- ⁶T. M. Rice and M. Sigrist, *J. Phys.: Condens. Matter* **7**, L643 (1995).
- ⁷M. K. Wu, D. Y. Chen, F. Z. Chien, S. R. Sheen, D. C. Ling, C. Y. Tai, C. Y. Tseng, D. H. Chen, and F. C. Zhang, *Z. Phys. B* **102**, 37 (1997).
- ⁸S. Nakatsuji, S. Ikeada, and Y. Maeno, *J. Phys. Soc. Jpn.* **66**, 1868 (1997).
- ⁹G. Cao, S. McCall, M. Shephard, J. E. Crow, and R. P. Guertin, *Phys. Rev. B* **56**, R2916 (1997).
- ¹⁰Q. Huang, J. L. Soubeyroux, O. Chmaissem, I. Natali Sora, A. Santoro, R. J. Cava, J. J. Krajewski, and W. F. Peck, Jr., *J. Solid State Chem.* **112**, 355 (1994); M. K. Crawford, M. A. Subramanian, R. L. Harlow, J. A. Fernandez-Baca, Z. R. Wang, and D. C. Johnston, *Phys. Rev. B* **49**, 9198 (1994).
- ¹¹M. A. Subramanian, M. K. Crawford, R. L. Harlow, T. Ami, J. A. Fernandez-Baca, Z. R. Wang, and D. C. Johnston, *Physica C* **235-240**, 743 (1994).
- ¹²M. Braden, H. Moudden, S. Nishizaki, Y. Maeno, and T. Fujita, *Physica C* **273**, 248 (1997).
- ¹³M. Braden, W. Reichardt, S. Nishizaki, Y. Mori, and Y. Maeno, *Phys. Rev. B* **57**, 1236 (1998).
- ¹⁴M. Braden, W. Paulus, A. Cousson, P. Vigoureux, G. Heger, A. Gukasov, P. Bourges, and D. Petitgrand, *Europhys. Lett.* **25**, 625 (1994).
- ¹⁵B. Grande, H. K. Müller-Buschbaum, and M. Schweizer, *Z. Anorg. Chem.* **428**, 120 (1977).
- ¹⁶R. J. Birgeneau and G. Shirane, in *Physical Properties of High Temperature Superconductors I*, edited by D. M. Ginsberg (World Scientific, Singapore, 1989); J. D. Axe, H. Moudden, D. Hohlwein, D. E. Cox, K. M. Mohanty, A. R. Moodenbough, and Youwen Xu, *Phys. Rev. Lett.* **62**, 2751 (1989); T. Suzuki and T. Fujita, *Physica C* **159**, 111 (1989).
- ¹⁷H. T. Stokes and D. M. Hatch, *Isotropy Subgroups of the 230 Crystallographic Space Groups* (World Scientific, Singapore, 1988).
- ¹⁸J. Rodriguez-Carvajal, *Abstracts of the Satellite Meeting on Powder diffraction of XVth Congr. Int. Union of Crystallography (IUCR, Toulouse, 1990)*, p. 127; J. Rodriguez-Carvajal, M. T. Fernandez-Diaz, and J. L. Martinez, *J. Phys.: Condens. Matter* **3**, 3215 (1991); J. Rodriguez-Carvajal, *Physica B* **152**, 55 (1993).
- ¹⁹T. Kiyama, K. Yoshimura, K. Kosuge, Y. Ikeda, and Y. Bando, *Phys. Rev. B* **54**, R756 (1996).
- ²⁰R. J. Cava, B. Batlogg, K. Kiyono, H. Takagi, J. J. Krajewski, W. F. Peck, Jr., L. W. Rupp, Jr., and C. H. Chen, *Phys. Rev. B* **49**, 11 890 (1994).
- ²¹S. A. Carter, B. Batlogg, R. J. Cava, J. J. Krajewski, W. F. Peck, Jr., and L. W. Rupp, Jr., *Phys. Rev. B* **51**, 17 184 (1995).
- ²²M. Braden and W. Reichardt (unpublished).
- ²³T. Vogt and D. J. Buttrey, *Phys. Rev. B* **52**, 9843 (1995).
- ²⁴P. G. Radaelli, D. E. Cox, M. Marezio, and S.-W. Cheong, *Phys. Rev. B* **55**, 3015 (1996).
- ²⁵A. D. Bruce and R. A. Cowley, *Structural Phase Transitions* (Taylor and Francis, London, 1981).
- ²⁶M. Braden, P. Schweiss, G. Heger, W. Reichardt, Z. Fisk, K. Gamayunov, I. Tanaka, and H. Kojima, *Physica C* **223**, 396 (1994).
- ²⁷M. K. Crawford, R. L. Harlow, E. M. McCarron, W. E. Farneth, N. Herron, H. Chou, and D. E. Cox, *Phys. Rev. B* **47**, 11 623 (1993).
- ²⁸M. T. Fernandez-Diaz, J. Rodriguez-Carvajal, J. L. Martinez, G. Fillion, F. Fernandez, and R. Saez-Puche, *Z. Phys. B* **82**, 275 (1991).
- ²⁹P. J. Brown, in *International Tables for Crystallography*, edited by A. S. C. Wilson (Kluwer Academic, Dordrecht, 1992).
- ³⁰J. B. Goodenough, *Magnetism and Chemical Bond* (Interscience, New York, 1963).
- ³¹P. Vigoureux, M. Braden, A. Gukasov, W. Paulus, P. Bourges, A. Cousson, D. Petitgrand, J. P. Lauriat, M. Meven, S. N. Barilo, D. I. Zhigunov, P. Adelman, and G. Heger, *Physica C* **273**, 239 (1997).
- ³²S. Ikeada, Y. Maeno, H. Muranashi, and T. Fujita, *J. Low Temp. Phys.* **105**, 1599 (1996); G. Cao, S. McCall, J. E. Crow, and R. P. Guertin, *Phys. Rev. B* **56**, 5387 (1997); G. Cao, S. McCall, J.

- E. Crow, and R. P. Guertin, *ibid.* **56**, R5740 (1997); S. Ikeda, Y. Maeno, and T. Fujita, *ibid.* **57**, 978 (1998).
- ³³K. K. Singh, P. Ganguly, and J. B. Goodenough, *J. Solid State Chem.* **52**, 254 (1984).
- ³⁴J. B. Goodenough, *MRS Bull.* **XV** (5), 23 (1990).
- ³⁵I. D. Brown and D. Altermatt, *Acta Crystallogr., Sect. A: Cryst. Phys., Diffr., Theor. Gen. Crystallogr.* **32**, 751 (1976).
- ³⁶J. D. Jorgensen, B. Dabrowski, Shiyou Pei, D. G. Hinks, L. Soederholm, B. Morosin, J. E. Schirber, E. L. Venturini, and D. S. Ginley, *Phys. Rev. B* **38**, 11 337 (1988); P. Zolliker, D. E. Cox, J. B. Parise, E. M. McCarron, and W. E. Farneth, *ibid.* **42**, 6332 (1990); D. Vaknin, J. L. Zarestky, D. C. Johnston, J. E. Schirber, and Z. Fisk, *ibid.* **49**, 9057 (1994).
- ³⁷D. J. Buttrey, P. Ganguly, J. M. Honig, C. N. Rao, R. R. Schartman, and G. N. Subbanna, *J. Solid State Chem.* **74**, 233 (1988); T. Kajitani, S. Hosoya, M. Hirabashi, T. Fukuda, and T. Onuzuka, *J. Phys. Soc. Jpn.* **58**, 3616 (1989); D. J. Buttrey, J. D. Sullivan, G. Shirane, and K. Yamada, *Phys. Rev. B* **42**, 3944 (1990).
- ³⁸B. Büchner, M. Braden, M. Cramm, W. Schlabitz, W. Schnelle, O. Hoffels, W. Braunisch, R. Müller, G. Heger, and D. Wohlleben, *Physica C* **185–189**, 903 (1991); M. K. Crawford, R. L. Harlow, E. M. McMarron, W. E. Farneth, J. D. Axe, H. Chou, and Q. Huang, *Phys. Rev. B* **44**, 7749 (1991); B. Büchner, M. Cramm, M. Braden, W. Braunisch, O. Hoffels, W. Schnelle, A. Freimuth, G. Heger, D. I. Khomskii, and D. Wohlleben, *Europhys. Lett.* **21**, 953 (1993).
- ³⁹M. Sera, M. Maki, M. Hiroi, N. Kobayashi, T. Suzuki, and T. Fukase, *Phys. Rev. B* **52**, R735 (1995).
- ⁴⁰S. Nakatsuji and Y. Maeno (unpublished).
- ⁴¹P. G. Radaelli, J. D. Jorgensen, A. J. Schulz, B. A. Hunter, J. L. Wagner, F. C. Chou, and D. C. Johnston, *Phys. Rev. B* **48**, 499 (1993).
- ⁴²J. D. Jorgensen, B. Dabrowski, Shiyou Pei, D. R. Richards, and D. G. Hinks, *Phys. Rev. B* **40**, 2187 (1989).
- ⁴³J. Zanen, G. A. Sawatski, and J. W. Allen, *Phys. Rev. Lett.* **55**, 418 (1985).
- ⁴⁴M. F. Hundley, J. D. Thompson, S. W. Cheong, Z. Fisk, and J. E. Schirber, *Phys. Rev. B* **41**, 4062 (1990).
- ⁴⁵J. B. Torrance, P. Lacorre, A. I. Nazzal, E. J. Ansaldo, and Ch. Niedermayer, *Phys. Rev. B* **45**, 8209 (1991); J. Rodriguez-Carvajal, S. Rosenkranz, M. L. Medarde, P. Lacorre, M. T. Fernandez-Diaz, F. Fauth, and V. Trounov, *ibid.* **57**, 456 (1998); M. L. Medarde, *J. Phys.: Condens. Matter* **9**, 1679 (1997).
- ⁴⁶D. B. McWhan, J. P. Remeika, T. M. Rice, W. F. Brinkmann, J. P. Maita, and A. Menth, *Phys. Rev. Lett.* **27**, 941 (1971).
- ⁴⁷J. J. Randall and R. Ward, *J. Am. Chem. Soc.* **81**, 2629 (1959).
- ⁴⁸T. C. Gibb, R. Greatrex, N. N. Greenwood, and P. Kaspi, *J. Chem. Soc. Dalton Trans.* **1973**, 1253 (1973).